JOURNAL OF GEOPHYSICAL RESEARCH, VOL. 96, NO. B4, PAGES 6321–6333, APRIL 10, 1991

Dispersion of P Waves in Subducted Lithosphere: Evidence for an Eclogite Layer

DAVID GUBBINS

Department of Earth Sciences, University of Leeds, Leeds, United Kingdom

ROEL SNIEDER

Department of Theoretical Geophysics, University of Utrecht, Utrecht, Netherlands

Cold, subducted lithosphere has relatively fast seismic velocity which leads to early arrivals for some event-station paths. The effect is very large for events in the Tonga-Kermadec deep seismic zone recorded at certain New Zealand stations. These particular arrivals are very high-frequency (3 Hz or greater) and sometimes resemble two distinct phases, the later arrival appearing at about the time predicted by Jeffreys-Bullen tables. Data from the digital station SNZO in Wellington confirm the travel time results of the analog stations and furthermore show frequencies above 5 Hz, much higher than can be seen on analog records, and up to 4% dispersion in the range 1–8 Hz. Energy in the second phase (which is often absent at SNZO) is mainly 1–2 Hz. The digital data support the idea, proposed earlier, that the effect is caused by propagation through a thin slab which passes only short-wavelength waves. The essential features of the wave propagation are modeled by acoustic waves in a one-dimensional high-velocity slab; the waveforms produced by the model are discussed in terms of the leaky modes of the system and calculated by a reflectivity method. A very thin (< 15 km) uniform slab provides the required dispersion, but the waves are heavily attenuated and would never be observed at teleseismic distances; a thicker slab allows the energy through but does not give enough dispersion. Altering the variation of velocity across the slab provides the required dispersion if a thick high-velocity layer, with wave speed increasing gradually with height, is overlain by a thin lid of even higher velocity. For the models considered the lid thickness must lie in the range 6–15 km and be continuous from a depth of about 50 km to the bottom of the earthquake zone. The thick layer could arise from the thermal anomaly in the subducted lithosphere; the thin lid may be the gabbroic part of the subducted crust that has transformed to eclogite.

INTRODUCTION

Deep seismic zones occur when a subducting plate descends into the mantle. The plate gradually warms and undergoes mineralogical phase changes as it descends; reviews of simple thermal models are given by *Sleep* [1973], and models of the mineralogy are given by *Ringwood* [1982] and *Helffrich et al.* [1989]. Seismological studies of subducted slabs have involved source mechanisms (for example, see *Giardini and Woodhouse* [1984] for the Tonga-Kermadec zone discussed in this paper); phase conversions at the interface between the slab and surrounding mantle [*Snoke et al.*, 1977; *Fukao et al.*, 1978; *Nakanishi*, 1980; *Nakanishi et al.*, 1981; *Matsuzawa et al.*, 1986]; propagation effects such as travel time anomalies [*Davies and McKenzie*, 1969]; and focusing effects of the slab [*Davies and Julian*, 1972]. Recent work on tomographic inversion for the P wave speed in the subduction zone has included refinement of the source locations [e.g., *Spencer and Gubbins*, 1980; *Creager and Jordan*, 1984; *Engdahl and Gubbins*, 1987]. In many of these studies the fast zone becomes very thin and in most cases the width is limited by the coarse parameterization of the velocity model. The fast zone may be so thin that ray theory breaks down and frequency-dependent wave propagation may occur. *Vidale* [1987] has used a finite difference method to compute seismograms for waves that have passed through typical slab structures, and *Cormier* [1989] has computed diffraction effects from slab structures using a Gaussian beam method, but otherwise rather little has been done with full wave theory.

Ansell and Gubbins [1986], hereinafter referred to as AG, studied some remarkable arrivals at stations in the New Zealand network. Waves from events in the Tonga-Kermadec deep seismic zone exhibit residuals in excess of 10 s relative to Jeffreys-Bullen (JB) tables and the appearance of two distinct P phases: an early, high-frequency, arrival and a later phase, with lower frequency, arriving at about the JB time. Figure 1 gives a map of the region and shows the geometry. AG's results can be summarized as follows:

1. Stations on the east of the North Island of New Zealand and the northern end of South Island (their zone 3) exhibit the fast double arrivals. The corresponding ray paths lie close to the subducted slab for most of their length due to a fortuitous bend in the zone.

2. Stations on the west side of North Island (their zones 1 and 2) are either slow relative to JB (showing that early arrivals on the east side are not simply caused by bias in the travel time curve) or are heavily attenuated by passage through the Taupo volcanic zone.

3. Arrivals throughout the rest of South Island (their zone 4) give variable results.

4. Counting peaks suggests the early phase has a dominant frequency of 3 Hz, but the analog recording system may mask higher frequencies.

Paper number 90JB02741.
0148-0227/91/90JB-02741$05.00

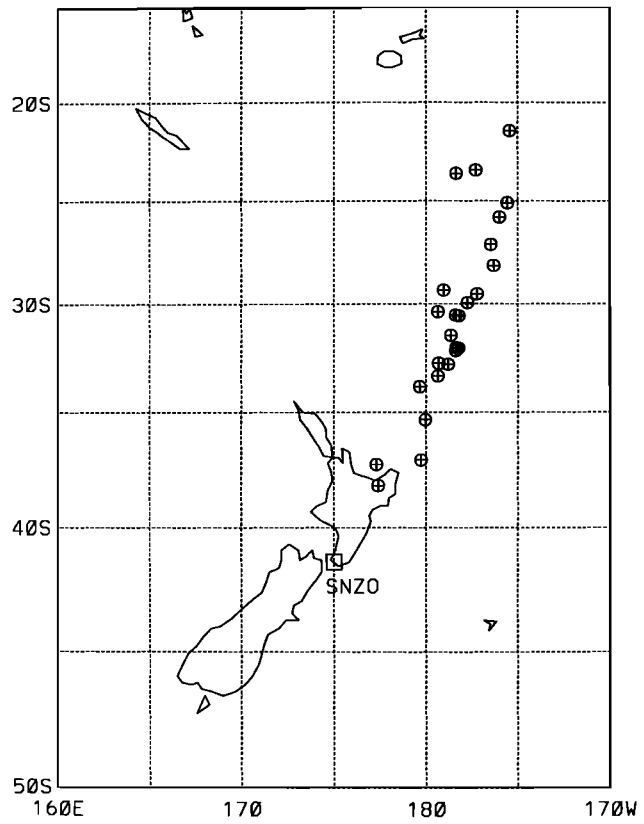

Fig. 1. Events used for this study. SNZO is a standard SRO site near Wellington, New Zealand.

5. At Wellington, where two phases are seen frequently, two seismometers have operated side by side. The Willmore has good high-frequency response and records the early phase well, but the other seismometer, a Benioff with poorer high-frequency response, does not record it. Comparison of the known frequency responses of the two instruments suggests the early phase has dominant frequency well above 3 Hz.

These results were interpreted as slab effects: the thin slab allows short-wavelength waves to travel at the high-velocity but the longer wavelengths do not "see" the slab and travel at normal mantle speed. Slow arrivals in zone 1 have passed through the slow wedge above the slab; variable arrivals in the south have left the slab and been subjected to a variety of attenuation and scattering effects so that sometimes the two-phase nature of the arrival is preserved and sometimes the early phase is lost.

AG's study was limited by the data quality, which was restricted by analog recording. Estimating high frequency by counting peaks is very unsatisfactory, and result (5) above, from Wellington, suggests very high frequencies are present that cannot be seen on the paper record. Digital recording is required for a more quantitative study. The instruments of the New Zealand network are now being replaced and digital records will eventually become available. In this preliminary study we use the only existing digital station (SNZO), the Seismic Research Observatory (SRO) site at Wellington. It has only one short-period, vertical component, instrument, the filter is not good for our purpose, and there are problems with the trigger so the first few seconds of the arrival are often lost, but these inadequacies are compensated for to some extent by the quiet borehole installation and large dynamic range of the digital recording system.

The Wellington site is relatively noisy compared with some other North Island stations such as Mangahao (MNG), and it is not as well placed relative to the slab to observe these early arrivals. JB residuals at the Willmore seismometer from suitable sources show a bimodal distribution with one peak around the JB time and one about 4 s early, suggesting the early phase is often missed altogether: the distribution at the quieter site of MNG has a single peak several seconds early (AG). JB residuals for WEL from the International Seismological Centre (ISC) Bulletin are shown in Table 1, which can be compared with the similar table for MNG given by AG. The largest residuals are from events in the latitude range 25–35°S above depth 300 km or thereabouts, depending on latitude. The pattern is similar for many New Zealand sites. Ray tracing confirms that the corresponding ray paths lie 10–50 km below the surface defined by the deep earthquakes, supporting the view that the anomaly is caused by fast subducted lithosphere. Station SNZO is only a few kilometers from Wellington (WEL) and should exhibit a similar pattern.

We approach the digital data with four specific questions in mind:

1. How high is the frequency of the early arrival?
2. Does the high-frequency continue to arrive in late parts of the wave train or does it have the form of an isolated pulse?
3. Are there two distinct phases or a dispersed wave train?
4. What kind of structures are responsible for the observed precursor?

Fast Arrivals at the Wellington SRO Station SNZO

Data were selected using the National Earthquake Information Center (NEIC) CD-roms distributed by the Orfeus data center. The archive includes all events above magnitude 5.5 from 1980 to 1984. Suitable events were selected from the latitude-longitude box 20°–40°S, 170°E–170°W. The search yielded twenty-eight events, three of which were unsuitable because the SNZO instrument triggered late (this only became apparent after scrutiny of the record). Twenty-five events remained; their hypocenters are listed in Table 2. They cover the full range of events discussed by AG; three are deep events, some at the extreme north of the zone where the early phase is observed, and several very close events.

The short-period record was plotted for each event, the time of the first arrival picked, and the residual relative to JB travel time tables calculated. The result was found to agree, to a few tenths of a second, with the residual published by the ISC for WEL or SNZO (in this time window, ISC appears to report WEL in preference to SNZO unless the former station fails to record). The results, shown in Table 2, confirm the findings of AG for other stations in the region. The residuals are somewhat smaller than for MNG but still exceed 10 s in two cases. The long-period trace showed no evidence of a precursor, and often the arrival was late relative to Jeffreys-Bullen times. These records were not used.

Each trace was filtered to extract specific frequency bands. Results for event 13 are shown in Figure 2. A high-pass causal filter with corner frequency at 2 Hz gives the

TABLE 1. ISC Residuals for Station WEL from 1964 to 1974

Latitude	Depth						
	0 km	100 km	200 km	300 km	400 km	500 km	600 km
15°S	-1.1(32)	-0.3(4)	-2.4(4)	–	-2.6(3)	–	–
16°S	-1.9(21)	-3.3(1)	-3.0(1)	-3.0(1)	-2.3(2)	–	–
17°S	-2.1(3)	-1.8(3)	-1.8(2)	–	-2.6(1)	-2.0(24)	-2.2(6)
18°S	1.8(3)	-0.5(4)	-0.8(2)	-2.4(2)	-2.4(2)	-1.7(5)	-1.0(4)
19°S	0.1(6)	-1.7(4)	-1.2(8)	-0.8(2)	-2.1(1)	-1.6(5)	-2.2(3)
20°S	-0.9(11)	-4.4(6)	-0.4(7)	-2.1(1)	-0.2(3)	-2.0(10)	-2.1(10)
21°S	1.3(19)	-2.1(5)	-1.0(5)	0.6(3)	-1.1(3)	-1.8(14)	-2.3(14)
22°S	-1.9(11)	-1.5(3)	-2.8(1)	–	-1.8(1)	-1.9(9)	-1.3(1)
23°S	-2.9(9)	-1.6(6)	–	-1.3(1)	-0.7(2)	-0.2(10)	–
24°S	-1.5(5)	0.7(5)	–	-1.8(1)	-1.4(5)	–	–
25°S	-6.8(2)	-3.7(2)	-1.6(1)	-1.8(1)	-0.8(2)	–	–
26°S	-1.5(3)	-3.6(3)	8.3(1)	–	-3.8(1)	–	–
27°S	-1.9(8)	-3.3(3)	–	-4.5(1)	–	–	–
28°S	-1.1(4)	-9.6(2)	–	-5.1(1)	–	–	–
29°S	-3.6(15)	-5.8(1)	-6.1(2)	–	–	–	–
30°S	-1.6(20)	–	-7.1(2)	-4.8(3)	–	–	–
31°S	-0.8(10)	–	-6.8(2)	-4.4(4)	–	–	–
32°S	-3.5(10)	-4.1(1)	-5.6(1)	–	–	–	–
33°S	-6.6(9)	–	–	–	–	–	–
34°S	-3.2(2)	–	–	–	–	–	–
35°S	-4.8(1)	-4.1(1)	–	–	–	–	–
36°S	-2.0(4)	–	–	–	–	–	–
37°S	-3.4(3)	–	–	–	–	–	–
38°S	-1.8(2)	-1.3(1)	–	–	–	–	–
39°S	2.5(1)	0.1(1)	–	–	–	–	–
40°S	–	–	–	–	–	–	–
41°S	2.1(4)	–	–	–	–	–	–

Time anomalies are relative to Jeffreys-Bullen travel time tables. The numbers in parentheses denote the number of observations in each latitude-depth cell. Very fast arrivals occur for depths < 300 km and the latitude range 25°–35°S.

clearest signal and makes the pick easier. A lowpass causal filter with a corner frequency at 1 Hz was used to search for "normal" arrivals: one appears on the second trace in Figure 3 about 2 s before the JB time. At these close distances the seismogram can be quite complex even for a simple Earth model. The theoretical arrivals were calculated for model PREM and compared with the lowpass-filtered traces to search for conventional second arrivals. In many cases the first significant energy was a depth phase pP or sP, and one is marked in Figure 2 (trace $f < 1$ Hz).

TABLE 2. Events Used for the Study of Digital Data

Δ°	JB,s	r_0, km	Latitude	Longitude	Depth, km	M_b	Event	Year	Month	Day	Hour	Minutes	Seconds
21.47	-4.0*	596	-21.466	-175.451	68.0	6.3	16	1983	3	21	7	44	17.79
19.02	-5.2*	513	-23.466	-177.297	79.0	6.7	3	1980	4	13	18	4	31.90
18.56	-4.1*	592	-23.627	-178.368	336.0	5.9	20	1984	1	19	16	15	16.74
18.08	-11.1*	322	-25.096	-175.569	37.0	5.9	13	1982	3	7	15	41	57.11
17.15	-7.0*	287	-25.795	-176.014	26.8	6.4	26	1984	9	28	0	3	35.46
15.90	-8.5*	260	-27.134	-176.474	27.0	5.5	6	1980	12	2	13	17	3.30
15.04	-8.7	218	-28.159	-176.320	30.7	5.6	19	1983	7	28	1	40	33.32
13.47	-9.7	191	-29.516	-177.228	33.0	5.6	10	1981	11	18	17	37	48.71
12.99	-8.2*	394	-29.335	-179.039	323.0	6.0	8	1981	9	28	17	56	18.09
12.90	-7.6*	191	-29.934	-177.741	33.0	6.1	11	1981	12	26	17	5	32.52
12.15	-9.7	170	-30.573	-178.208	33.0	5.7	7	1981	3	7	23	30	8.40
12.12	-2.6	172	-30.536	-178.375	33.0	5.5	27	1984	10	19	19	59	56.24
11.92	-8.5*	288	-30.383	-179.339	238.0	6.0	15	1983	1	26	16	2	21.35
11.16	-11.2	159	-31.485	-178.660	79.0	6.0	14	1982	3	28	3	52	34.59
10.77	-6.6*	132	-32.068	-178.370	33.0	5.7	23	1984	9	17	9	8	52.73
10.74	-9.0	131	-32.091	-178.235	33.0	5.5	24	1984	9	22	10	15	16.06
10.65	-5.5	128	-32.204	-178.376	33.0	5.5	25	1984	9	22	11	43	16.51
9.93	-8.2	116	-32.835	-178.791	45.8	5.6	18	1983	6	25	10	3	17.42
9.76	-5.4	110	-32.788	-179.306	33.0	5.6	21	1984	8	4	14	59	34.36
9.22	-3.8	90	-33.380	-179.348	33.0	6.0	22	1984	8	30	16	6	13.92
8.40	-7.0	81	-33.866	179.649	25.2	5.8	17	1983	5	5	4	43	50.46
7.28	-6.0	79	-35.346	179.960	33.0	5.7	1	1980	11	29	6	48	46.90
5.72	-4.4	51	-37.112	179.712	34.6	5.7	9	1981	12	1	17	46	43.71
4.48	-2.0	48	-37.307	177.301	33.0	5.7	2	1981	3	5	12	53	29.50
3.72	-0.3	68	-38.220	177.399	68.2	5.9	28	1984	3	8	0	40	47.89

Events are arranged in order of distance from the station SNZO. Numbering order is arbitrary. Δ° is the distance, JB is the Jeffreys-Bullen residual, LF is the time of a second low-frequency phase relative to JB (when one was observed), and, and r_0 is the maximum depth of the ray path. Latitude and longitude are measured in degrees and the minus signs indicate south and west respectively.

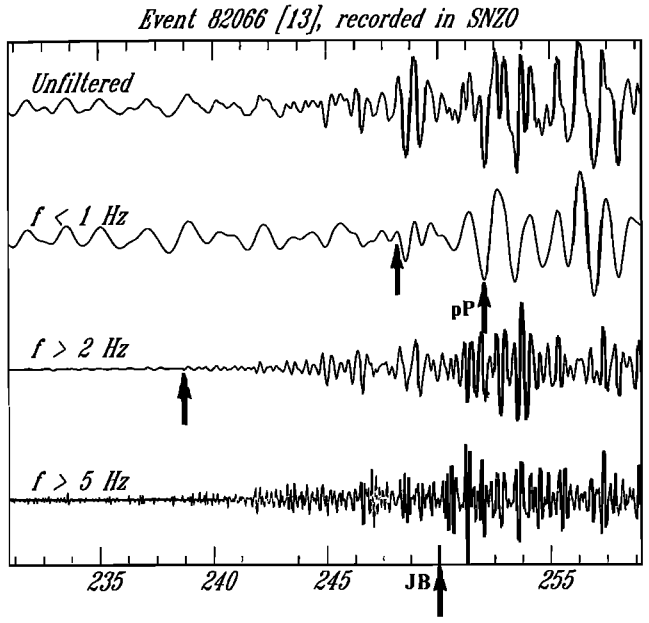

Fig. 2. Short-period vertical component seismograms for an event in the Tonga deep seismic zone (event 13 in Table 2). Traces are: the SRO short-period response, one lowpass filtered with a corner frequency of 1 Hz, one highpass filtered with a corner frequency of 2 Hz, and one highpassed with a corner frequency of 5 Hz. Picks are shown for the first arrival, JB travel time, low-frequency "second arrival", and depth phase.

The fourth trace in Figure 2 shows the result of a highpass filter with corner frequency at 5 Hz. The clear arrival shows that the precursor contains very high-frequency indeed. In this study the upper limit of the observed frequency is often set by the instrument response and the sampling rate (20 times per second). This suggests an instrument more sensitive to high-frequency would yield better information.

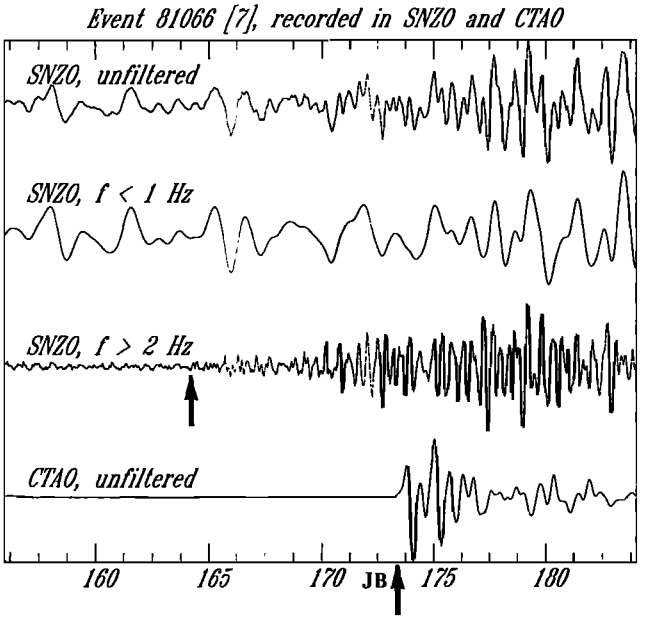

Fig. 3. Short-period seismograms for event 7 in Table 2; as in Figure 2 except for the last which shows the short-period vertical component seismogram at the SRO CTAO in Charters Towers, Australia; the simple waveform shows the complexity at SNZO is a path and not a source effect. The P arrival of the CTAO record is aligned with the JB time of the SNZO record.

Event 7 is shown in Figure 3. Here the lowpass arrival is very difficult to detect, although energy clearly begins to arrive about 2 s after the JB time and builds to significantly above the noise by 185 s. Note that the arriving wave recorded at SNZO does not have an impulsive character but rather builds up slowly to an extended wave train. This is not the case at other stations for the same event. The bottom trace in Figure 3 shows the recording of the same event at a second station, CTAO, in Australia. The waveform is very clean and impulsive, showing the complexity of the arrival at SNZO is a path and not a source effect.

All events were studied and arrivals picked, where possible, on both highpass and lowpass traces. The picks were based on amplitude rather than frequency changes. The high-frequency results reproduced the picks of the original records; a low-frequency pick was often impossible. The results confirm the general observation that a 1 Hz signal arrives near the JB time at SNZO.

From this study we conclude:

1. The initial phase includes frequencies above 5 Hz. It is remarkable that such high frequencies should survive long propagation paths in the mantle (up to 20°). *Der et al.* [1982] find that Q increases with increasing frequency and depends on tectonic setting. Furthermore, *Bache et al.* [1985] find that Q increases with frequency and is independent of mantle path above 3 Hz. "Normal" mantle may well have very low attenuation for high-frequency body waves.

2. The initial high-frequency is not in the form of a distinct pulse but continues well into the coda, indicating reverberations within structure along the path.

3. Later, low-frequency, arrivals do occur but are often submerged in the noise and may be confused with depth phases or other conventional second arrivals due to a layered crustal structure.

4. The JB travel time tables give a generally accurate prediction of the low-frequency arrival. The deep event 8 (Table 2) is an exception: this may reveal an inaccuracy in the tables for deep events, or mislocation.

5. The waveforms are a path rather than a source effect because other stations, such as CTAO, give clear impulsive arrivals.

These conclusions reinforce those made by AG and show that the frequency of the first arrival is even higher than could be measured on the analog recordings.

Evidence for Dispersion

Are there two distinct phases with different frequencies or a single dispersed wave train? Two phases can coexist within the framework of ray theory only if one ray propagates through the slab and the other propagates outside the slab independently. If the structure has significant variations on the length scale of the first Fresnel zone, the concept of ray theory breaks down and frequency-dependent effects, such as dispersion, become operative. For example, depth phases on these seismograms have relatively low-frequency (i.e., normal 1 Hz energy), they take off with a very different angle of incidence from the direct P wave, do not travel near the slab, and can therefore be regarded as rays independent of direct P. They do not exhibit dispersion. AG suggest that the P wave splits and part travels through the slab at high speed, retaining high frequencies, while the other part travels in "normal" mantle beneath the slab, losing high fre-

quencies by attenuation. This view of two distinct geometrical ray paths will be valid only if the width of the Fresnel zone of the rays is much smaller than the length scale of variation in the structure, otherwise the assumptions of geometrical optics breaks down. Any observed dispersion will indicate that this is indeed the case.

Dispersion will manifest itself in the seismograms by a gradual change in frequency in the precursor, with lower-frequency energy arriving after the first onset of high-frequency energy. It was impossible to discern any such dispersion in the analog records. We now examine the digital seismograms from SNZO for evidence of dispersion in the very early part of the waveform. Each waveform was filtered to pass the restricted frequency bands 0.5–1.5, 1.5–2.5, 2.5–3.5, 4.5–5.5, and 5.5–6.5 Hz, using a one-pass Bessel filter which is causal and therefore preserves the onset time of the signal. An example of the results is shown in Figure 4 for event 15, a deep event. Dispersion is clearly visible in the filtered traces. Most of it in this case occurs between 1 and 3 Hz.

An alternative way to display the dispersion is similar to the multiple-filter technique of *Dziewonski et al.* [1969], in which time windows are passed through a suite of zero-phase Gaussian filters with a range of frequencies and the resulting time-frequency window is contoured. The filters are acausal but the effect on the onset time of the signal is negligible. The plots in Figure 5 have been scaled to equalize the energy in each frequency band. Figure 5*f* corresponds to event 15 in Figure 4. Frequency is plotted along the horizontal axis, and time is plotted up the vertical axis for an interval slightly exceeding the length of the precursor. A vertical swath of Figure 5*f* centered on, for example, 3 Hz, gives the power in the band-passed trace centered on 3 Hz in Figure 4. The onset on each trace in Figure 4 can be seen to correspond to the start of significant energy in Figure 5*f*. The Gaussian filtering technique averages in time as well as frequency, so the time-frequency plots give only a smoothed estimate of the seismic energy. Dispersion appears in Figure 5*f* through

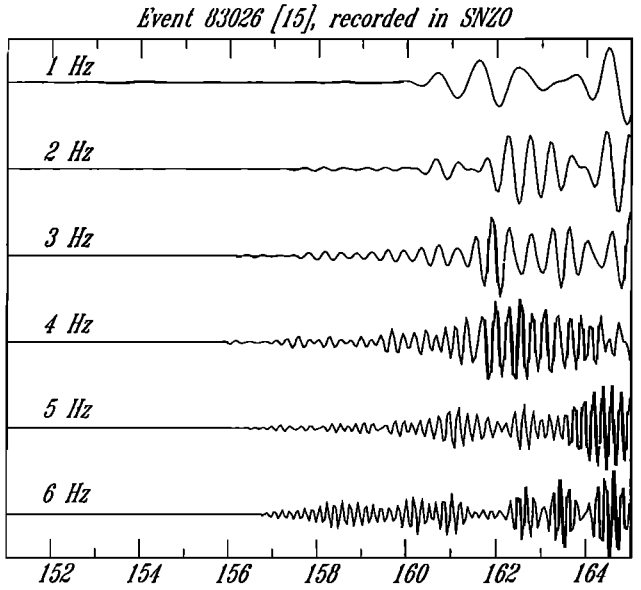

Fig. 4. Band-pass filtered traces for event 15. Each trace has a bandwidth of 1 Hz, centered on (from top down) 1, 2, 3, 4, 5, and 6 Hz.

lack of energy in the bottom left-hand corner of every plot. Figures 4*a* and 4*b* give events 13 and 7, for comparison with seismograms in Figures 2 and 3 respectively. Each show 3–4% dispersion. Events 11 and 26 in 5*c* and 5*d* give two more examples of shallow events with about 2% dispersion. The last pair, 3 and 15, are both deep events, with only 1% dispersion. Ray tracing for the latter two events shows that the waves pass below the deepest earthquakes in the zone and, presumably, leave the slab relatively quickly. The dispersion is correspondingly small.

This range of earthquakes shows that dispersion is always present, although the delay is not uniform with frequency. Most of the time-frequency plots suggest that the dispersion is prominent between 1 and 3 Hz; there are also "holes" in the arriving energy (at 3.5 Hz in event 15 and at 4 Hz, 168 s, in event 7 for example). This fine structure can arise from detailed layering in the subducted slab as explained in section 5, but no attempt has been made to model it. The energy arriving before the precursor at both low and high-frequency is noise. The dispersion is rather less than the JB residual or the burst of 1 Hz energy that is often seen on SNZO or the analog records.

Modeling of the Dispersion

These waves travel along the strike of the slab for a considerable distance. The variation in seismic velocity along the slab is assumed to be smooth, like that in normal mantle, and any possible sudden changes along the ray path, for example due to a break in the slab, are ignored. Velocity variations across the slab are, however, rapid because of the compositional anomalies and temperature perturbation associated with the subducted lithosphere. Under such conditions we can hope to separate the deflection of the propagation path caused by slow variations along the slab from dispersion caused by rapid variations across the slab and treat the wave field as a set of (leaky) modes propagating within the slab. The WKBJ approximation for guided waves [*Bretherton*, 1968] justifies this approach. We are interested only in the dispersion induced by rapid variations of properties across the slab, and not in the path of propagation along the slab. We therefore model the slab with a plane-layered medium. The data will undoubtedly contain complicated effects arising from any three-dimensional structure through which it passes, but general properties of the dispersion will depend predominantly on the structure across the path and the distance traveled through that structure.

We also choose to restrict the initial modeling to the acoustic case; no S waves are included. In this way we shall isolate dispersion effects on the P wave and eliminate complications in the synthetic seismograms associated with conversion to S. We do not expect conversion to be high or important because these waves travel at close-to-grazing incidence with the slab surfaces and because we are only interested in the first part of the waveform: any conversion to S wave energy will travel more slowly and will not arrive in the first few seconds. The acoustic calculation cannot account properly for amplitudes. Energy will be interchanged at interfaces by conversion to and from S and this will not be included in our synthetics. We therefore draw no conclusions from amplitudes or relative amplitudes in the synthetics. A more complete study of the elastic case is reserved for later work.

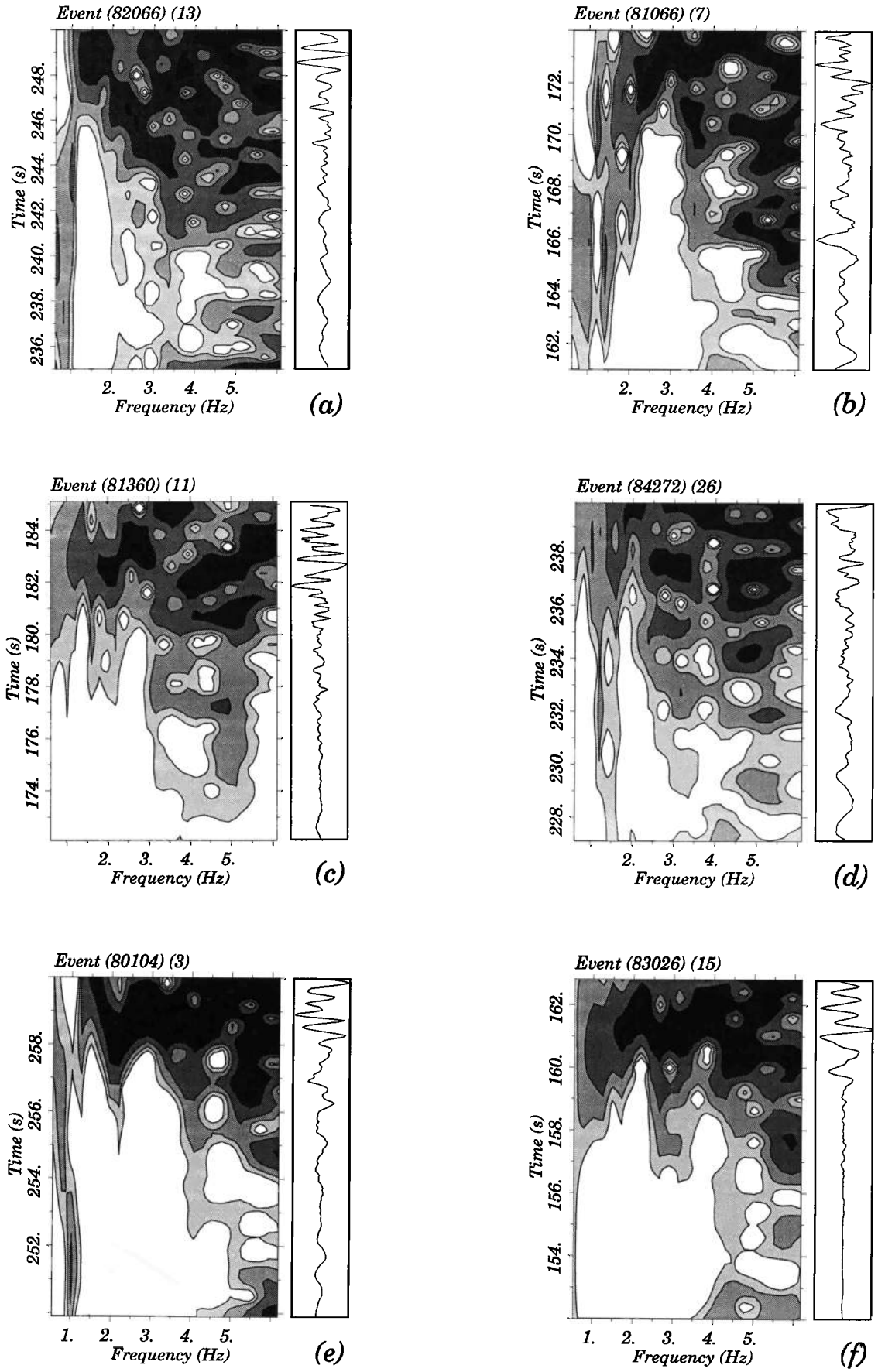

Fig. 5. Time-frequency plots for six different events showing dispersion. Compare the plot for event 15 with the band-passed traces in Figure 4.

Our simplest model is that of a high-velocity horizontal slab, with thickness H and wave speed c_1, embedded in an infinite medium with wave speed c_0. Both materials have density ρ. The acoustic case is equivalent to a fluid layer embedded in an infinite fluid medium. The source is placed at various heights within the slab at $x = 0$, where (x, z) are Cartesian coordinates with x horizontal and z downward, with the top of the layer at $z = 0$. Positioning of the source has a large effect on the amplitude of the response, but we do not wish to discuss this in the context of an acoustic model, which will not provide realistic amplitudes. The response is calculated at a horizontal distance L from the source and just above the slab.

First consider the modes of the system. Their frequencies are derived from the condition that energy radiates away from both upper and lower interface of the slab. The period equation, derived in the appendix, is

$$\tan \frac{\omega H}{d} i\gamma^{\frac{1}{2}} = \frac{2\gamma^{\frac{1}{2}}(1-\gamma)^{\frac{1}{2}}}{1-2\gamma} \tag{1}$$

where d is defined by (20) and γ by (21), which may be rewritten as

$$\frac{1}{c^2} = \frac{\gamma}{c_0^2} + \frac{(1-\gamma)}{c_1^2} \tag{2}$$

where $c = \omega/k$ is the phase speed of the mode.

Equation (1) determines γ and hence the phase velocity of the mode in terms of ωH. We are interested in high-frequency modes that propagate like body waves close to the phase speed of the fast slab. These modes have

$$\epsilon^{-1} = \frac{\omega H}{d} \gg 1$$

and $\gamma \ll 1$. Hence solutions of (1) exist with, to leading order in the small parameter ϵ,

$$\gamma^{\frac{1}{2}} = -\frac{in\pi d}{\omega H} \tag{3}$$

where n is an integer, the overtone number. The phase speed is, from (2),

$$c = c_1 \left(1 + \frac{n^2\pi^2 c_1^2}{2\omega^2 H^2}\right) \tag{4}$$

Note that the phase speed is higher than in either of the two media and is in this limit independent of c_0.

The group velocity is obtained from (4) by setting $k = \omega/c$, where k is the wave number, and differentiating with respect to ω. After some manipulation this gives, again to first order in ϵ,

$$c_g = c_1 \left(1 - \frac{n^2\pi^2 c_1^2}{2\omega^2 H^2}\right) \tag{5}$$

The group velocity is, as expected, slower than the wave speed in the faster medium, and it decreases with decreasing frequency: the high frequencies travel the fastest.

The wave number is real to this order in ϵ and there is no attenuation. Second-order terms must be considered in determining the imaginary part of the wave number. They give

$$k_i H = \frac{2n^2\pi^2 c_1}{\omega H} \frac{d}{\omega H} \tag{6}$$

The vertical wave number in the slab, η_1, is given asymptotically by

$$\eta_1 = \frac{i\gamma^{\frac{1}{2}}}{d} = \frac{n\pi}{\omega H} \tag{7}$$

which follows from (4) and (23). The wavelength for the n^{th} overtone is therefore $2H/n$: the modes are forced to fit into the slab.

Note that frequency appears everywhere multiplied by H, the slab thickness, so that reducing the slab thickness is equivalent to considering a lower frequency. Taking $c_0 = 8$ km s^{-1}, $c_1 = 8.4$ km s^{-1}, and a 5% velocity contrast between the slab and the surrounding medium, (5) gives a 1% difference between infinite frequency $\nu(= \omega/2\pi)$ and $\nu H \approx 30$ for $n = 1$, the fundamental, corresponding to 1 Hz waves and a slab thickness of 30 km. The small parameter, ϵ, is in this case 0.14. Equation (6) gives $k_i H = 0.125$, showing that the waves decay exponentially along the slab by a factor of e approximately every eight slab widths, or by a factor of 64 in a typical slab length of 1000 km (corresponding to angular distance 10°, typical of the events in Table 2) for 1 Hz waves and $H = 30$ km. The damping reflects the decay of 1 Hz energy relative to high-frequency energy and is severe.

We require more than 1% dispersion to explain the observations. Equation (5) gives 3% dispersion at 2 Hz, as required by the data, for an 8 km thick slab. For a 5% velocity contrast we have $\epsilon = 0.32$. However, the attenuation length is now much shorter, close to $2H$, or 16 km. These frequencies are therefore completely eliminated by passage along the slab; the attenuation factor at 2 Hz is $7\ 10^{-28}$ in 1000 km! The asymptotic approximation is not very accurate at this value of ϵ, but a numerical solution for the roots of (1) reinforces the conclusion of very heavy attenuation.

We conclude that although the uniform slab can produce the required dispersion if it is thin enough, the attenuation associated with leakage of energy out of the slab is so great that the waves would never be observed. This result is confirmed by the synthetic seismograms described in the next section.

Our model is a very simple one, and it might be argued that the slab will retain more energy in the real situation. However, there is everything to indicate the contrary: twists in the slab to a less ideal geometry would lose more energy; P-to-S conversions, not accounted for in the model, would also drain energy from the P wave.

The only aspect of the model we can adjust in order to satisfy the twin constraints of high dispersion and low attenuation is the profile of the slab. We are therefore forced to consider a more complicated structure in order to retain the energy inside the slab.

Modeling the Waveforms by a Simple Reflectivity Method

Consider a more complex slab structure. The same approach applies in the determination of leaky mode wave numbers, but the period equation must be solved numerically: we lose the simple analytical approach of the previous section. Furthermore, the frequency no longer scales simply with the slab thickness, although scale invariance with the total thickness of the slab remains. The derivation of the period equation becomes rather intricate and specialized to

each slab profile; it is more efficient to use a numerical reflectivity approach.

Consider a stack of N homogeneous plane layers with velocity c_n, density ρ_n and thickness H_n. The stack is surrounded on both sides by a homogeneous space with velocity c_0 and density ρ_0. An explosive source is present somewhere in the slab, and a radiation condition is imposed outside the slab. The generated wave field is computed using the reflectivity method [*Fuchs and Muller*, 1971]. The wave field is expressed as a double integral over slowness p and frequency ω:

$$u(r,z,t) = \Re \int_{-\infty}^{\infty} d\omega \int_{0}^{\infty} dp\, \mathcal{N}(\omega,p,z) \exp i\omega(pr - t) \quad (8)$$

where $\mathcal{N}$ has the form

$$\mathcal{N}(\omega,p,z) = \frac{G(\omega H_1\eta_1,\ldots,\omega H_N\eta_N,\rho_1,\ldots,\rho_N,p,z)}{\Delta(\omega H_1\eta_1,\ldots,\omega H_N\eta_N,\rho_1,\ldots,\rho_N,p)} \quad (9)$$

and $\Delta = 0$ is the period equation. In this expression, r is the distance along the slab (the length of the ray path), z is the distance from the receiver from the top of the slab, and η_n is given by

$$\eta_n = \left(\frac{1}{c_n^2} - p^2\right)^{\frac{1}{2}} \quad (10)$$

In the numerical examples presented in this paper, the slowness integral in (8) is performed by a straightforward numerical quadrature and the frequency integral is realized by a fast Fourier transform.

The integrand can be derived using propagator matrices [*Gilbert and Backus*, 1966]. The reader is referred to *Aki and Richards* [1980] for details concerning the reflectivity method and the use of propagators. The excitation of the wave field influences only the numerator G in (9), while the period function Δ in (9) depends only on the material properties of the medium. Assuming the frequency ω to be real, the zeroes of Δ on the real p axis correspond to trapped modes, while the zeroes on the unphysical Riemann sheet in the complex p plane correspond to leaky modes [*Watson*, 1972]. Note that the frequency and the layer thickness enter the integrand in the reflectivity integral (8) only in the dimensionless combination $\omega H_n\eta_n$. For the simplest case of a single layer with the same density ρ as the surrounding material and a source at the top of the layer, the wave field at a distance $-z$ from the top of the slab is given by

$$u(r,z,t) = -\Re e^{i\pi/4} \int_{-\infty}^{\infty}\int_{0}^{\infty} \mathcal{I}(p,\omega)d\omega dp \quad (11)$$

where

$$\mathcal{I} = \left(\frac{2\omega p}{\pi r}\right)^{\frac{1}{2}} \mathcal{N}(\omega,p)\, \rho e^{i\omega(pr-\eta_0 z-t)} \quad (12)$$

and

$$\mathcal{N}(\omega,p) = \frac{\eta_0 \sin\omega\eta_1 H + i\eta_1 \cos\omega\eta_1 H}{2\eta_0\eta_1 \cos\omega\eta_1 H - i(\eta_0^2+\eta_1^2)\sin\omega\eta_1 H} \quad (13)$$

The period equation (1) follows from setting the denominator in (13) to zero.

Numerical results for a uniform high-velocity slab were as predicted by the modal analysis in the previous section: no fast arrival could be seen for a thin slab, and no dispersion for a thick slab. We studied progressively more complicated models until the synthetics exhibited the main features seen in the data.

A second high-velocity layer was added to give a staircase structure as shown in Figure 6. The waves propagating in the surrounding medium arrive at 125 s. Those in the high-velocity lid and those in the bottom of the slab are visible as two distinct precursors (119 s and 122 s). The total thickness was kept at 60 km and the width of the upper lid, H, was varied. The lid was given velocity 8.4 km s^{-1}, the intermediate layer 8.2 km s^{-1}, and the surrounding medium 8.0 km s^{-1}. The resulting synthetic seismograms are shown in Figure 6. For $H \leq 6$ km there is no precursor arriving with the velocity of the lid: the energy is not retained, as with the case of a uniform slab. For $H \geq 20$ km there is no dispersion: energy of all frequencies arrives at the fast speed corresponding to the lid. At intermediate widths there is dispersion, as the time-frequency plots in Figure 7 show. The seismograms have the appearance of two distinct pulses rather than a dispersed wave train. The best compromise between dispersion and a substantial precursor is provided by the model with H =10 km.

A more complicated set of models had 10 layers to approximate a smooth velocity variation across the slab. A smooth structure is expected from the temperature variation in the subducted plate. The overall width of the fast zone is again kept at 60 km, and the high-velocity lid is varied in thickness. The lid has velocity 8.4 km s^{-1}, and the ramp varies from 8.0 to 8.33 km s^{-1}. The results are shown in Figure 8. When $H = 0$ (i.e., there is no lid) there is no dispersion, and most of the energy arrives at 8 km s^{-1}, showing that a fast lid is needed for dispersion in combination with the thicker, slower, zone to retain the energy. The precursor, traveling at the lid velocity, is virtually absent up to and including $H = 6$ km. There is almost no dispersion for $H \geq 15$ km (the energy propagates at the fast lid speed) and very little for $H > 10$ km. The synthetics with the most realistic dispersion are obtained with lid thicknesses of 8–10

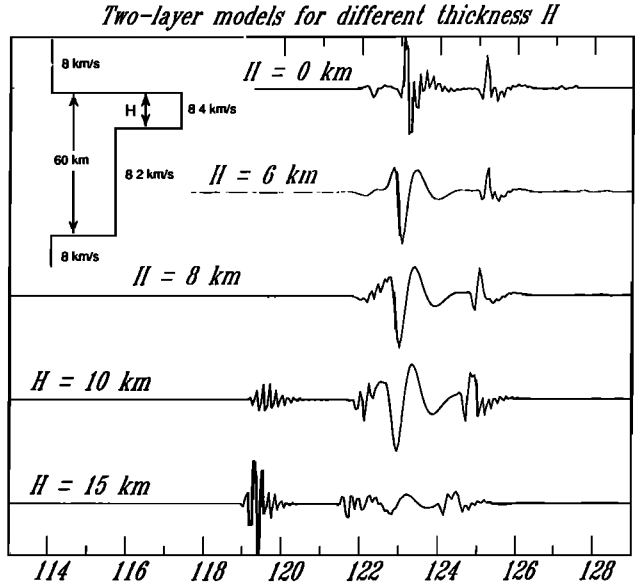

Fig. 6. Synthetic seismograms for two-layer models of the fast slab. Total thickness is 60 km; thickness of the high-velocity lid H varies. Note the appearance of three phases corresponding to the three velocities in the model.

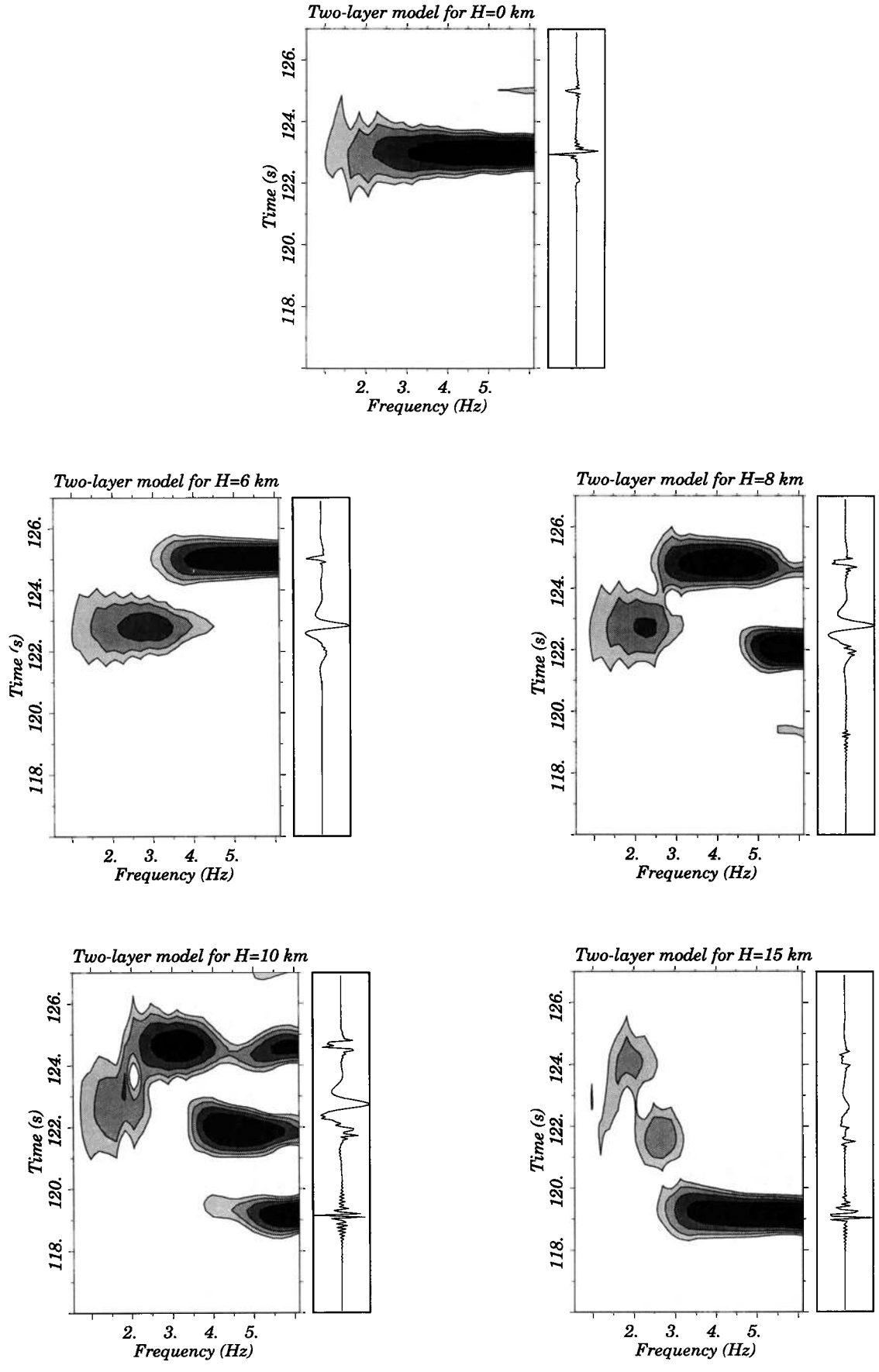

Fig. 7. Time-frequency plots corresponding to the synthetics in Figure 6.

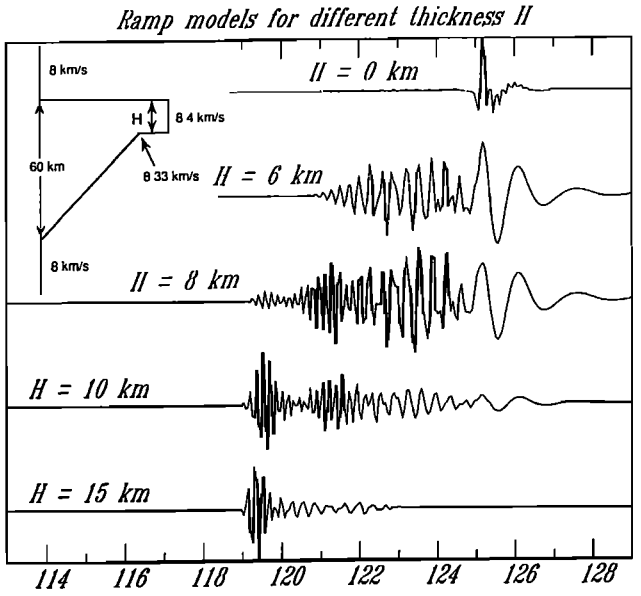

Fig. 8. Synthetic seismograms for ramp models. The smoothly varying base is represented by 10 layers. Note the appearance of a uniformly dispersed wave train and the absence of early high-frequency energy for $H = 0$ and $H = 6$ km.

km. The time-frequency plots in Figure 9 show dispersion rather than separate arrivals.

The two-layer models do not fit the data well because of the appearance of two distinct phases. However, three-dimensional structure along the slab may smear out these arrivals and produce a verisimilitude of dispersion in the real data, so that it is hard to discriminate between the two-layer and ramp models.

CONCLUSIONS

This study of digital data has given simple answers to the first two questions given in the introduction: the early signal is very high frequency, up to 8 Hz on this instrument, and it continues to arrive well into the wave train. The value of 8 Hz is based on an instrument with 20 times per second sampling, with a Nuyquist frequency of 10 Hz, and it is quite possible that even higher frequency energy is present. The third question, whether there is dispersion or two distinct phases, cannot be answered with the same clarity. The band-pass-filtered seismograms show 1–3% dispersion, which is rather less than both the JB residual (5–7%) and the time between first onset and the arrival of a second pulse of low-frequency energy (usually at about the JB time). This second pulse is not always present. We conclude the propagation path produces some dispersion, but that other effects may also be present to cause multipathing. The dispersion is considerably more severe than that studied by *Vidale* [1987] and *Vidale and Garcia-Gonzales* [1988] in broad slablike structures and demands a sharper variation in seismic velocity than they used.

The theory shows that a simple uniform fast slab cannot explain the observations because the energy leaks away. A more complicated structure is needed to retain the energy. A high-velocity thin lid above a thicker layer of slower velocity (but still faster than the surrounding mantle) produces essentially two arrivals, the first being confined to high-frequency, depending on the thickness of the lid. Alternatively, a high-velocity lid above a smoothly varying, slower-velocity layer (again faster than the surrounding mantle) produces the observed dispersion without the appearance of two distinct phases. The smooth model is preferred because it matches the seismograms best and is physically most plausible. With better data it might be possible to relate persistent "holes" in the time-frequency plots to layering in the subducted slab, but existing data does not justify any further interpretation. A firm result of the theory is the existence of a very thin high-velocity layer. The width is constrained by the model to lie between 6 and 15 km, probably between 8 and 10 km. The one-dimensional approximation may make this an overestimate, but the acoustic approximation is not believed to affect it since the wavelengths of acoustic and elastic waves are the same for a given velocity.

The acoustic approximation is unlikely to predict amplitudes accurately and we have avoided drawing conclusions based on amplitude. However, we believe source position relative to the slab to be critical in determining amplitudes in the real Earth, as it is in the acoustic calculations.

The same conclusions would apply to models with the high-velocity "lid" on the bottom rather than the top, but it is unlikely that such a high-velocity region should lie at the base of the subducted lithosphere; it is more plausible to have a thin layer on top. The lid has similar thickness to oceanic crust, much thinner than either the lithosphere or the width generally assumed for the fast seismic zone. Subducted gabbroic crust will have low seismic velocity; it must have transformed to eclogite in order to explain the observed high-velocity, and we think this is the most likely explanation of the high-velocity lid.

Helffrich et al. [1989] have performed theoretical calculations, using the Birch-Murnaghan law and experimental data from the laboratory, for the seismic velocities of materials at elevated pressure and temperature. They conclude that eclogite cannot produce the required velocity anomaly: they attribute only 0.5% to variation in composition and 1.75% to temperature effects in the slab. The thin top layer of the slab is expected to warm up relatively quickly and the temperature anomaly will be very small at depth. If these theoretical calculations are right, we must seek an alternative explanation for the high-velocity lid. Stress associated with subduction may cause mineral orientation of olivine in the mantle above the slab, producing anisotropy with the fastest direction aligned with the shear and the slowest direction normal to the slab [*McKenzie*, 1979]. This anisotropy will be difficult to distinguish from heterogeneity: seismic waves will be traveling horizontally near the deepest points on the ray and therefore more slowly from both the anisotropic effect and the decay in temperature anomaly with depth. The two effects arise from different regions, one in the top of the slab and one above the slab. Some more sophisticated observation, like shear wave splitting, is needed to discriminate between the two. We prefer the eclogite interpretation because of the similarity between the thickness of the lid and that of oceanic crust.

Dispersion requiring about 200 km of propagation through the fast layer is observed from two events below 300 km (events 8 and 20). Their ray paths lie close to the slab until the level of the deepest events, when, presumably, they pass out the bottom. The lid must therefore penetrate to at least 500 km. The dispersion could be caused by propagation beneath the receiver, but this would require energy to reenter the high-velocity lid after passage through

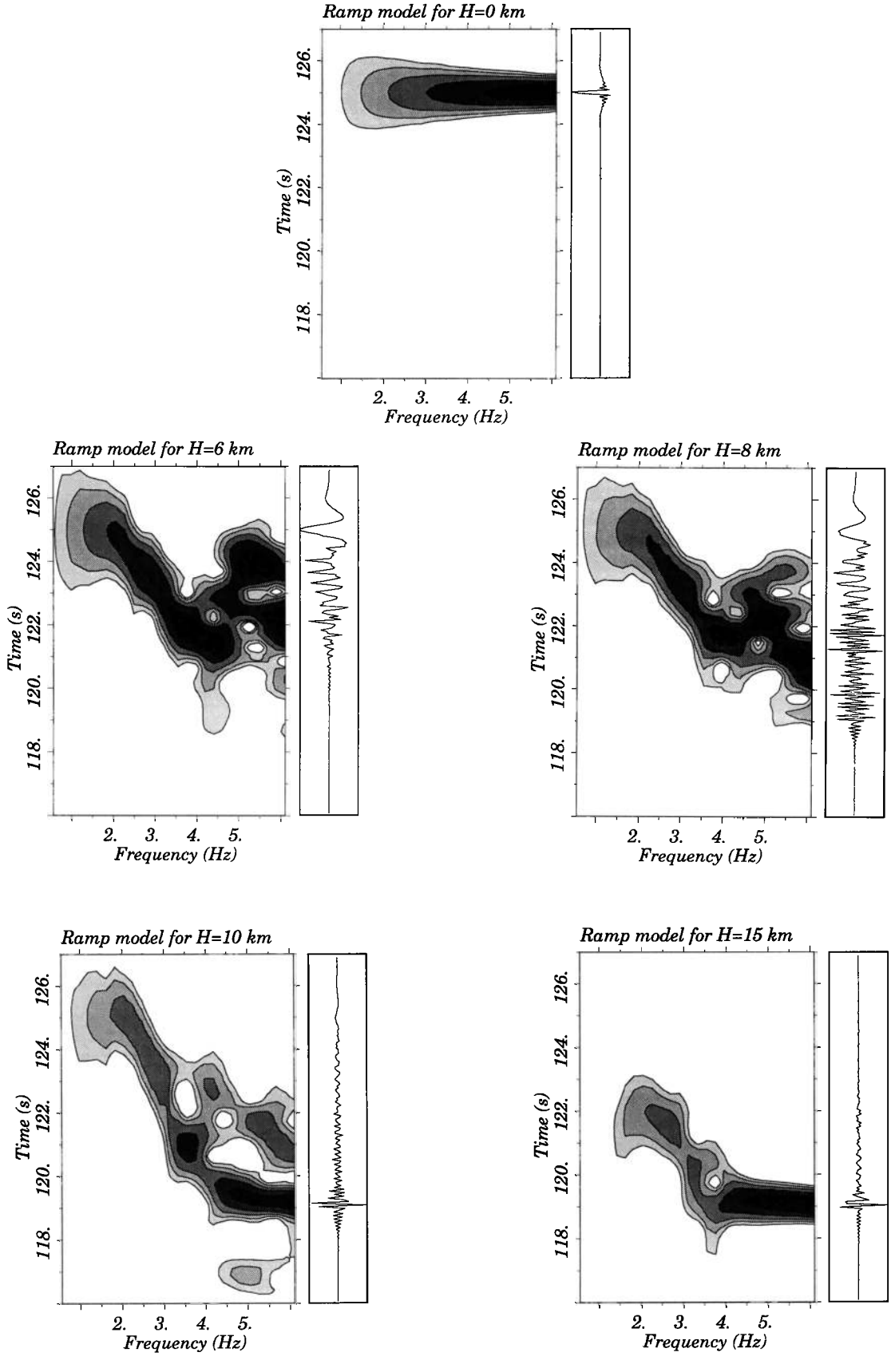

Fig. 9. Time-frequency plots for the ramp models. Note the even dispersion for the ramp models.

the mantle, which seems unlikely. This also means the lid must be continuous, without any breaks or faults, for the dispersion to be observed for so many events.

Our model is rather different from that of *Huppert and Frohlich* [1981], who studied arrivals from stations AFI and RAO, which lie above the Tonga-Kermadec slab, and preferred a fast lower region and thick slower lid, as expected from the temperature anomaly. It is possible their data could be explained by a model similar to ours, with the fast lid on top, but it seems implausible to have the very thin lid required by our data on the underside.

Converted phases require a sharp interface on the slab surface [*Fukao et al.*, 1978; *Matsusawa et al.*, 1986; *Nakanishi et al.*, 1981], and it is difficult to explain such a sharp contrast by temperature alone, because sharp temperature changes would diffuse away relatively quickly [*Sleep*, 1973; *Helffrich et al.*, 1989]. A basaltic layer would form a waveguide and propagate high-frequency energy at low seismic velocity. Such arrivals would be late and therefore difficult to detect in the seismograms studied in this paper, although the absence of a precursor for the closest events in Table 2 suggests the fast path is absent at shallow depths close to the receiver. Comparing residuals and deepest points on the ray paths in Table 2 shows that clear precursors are produced by structure at and 80 km. If the fast zone is eclogite the transformation from gabbro therefore occur above 80 km. This compares well with the results of *Hori et al.* [1985], who find evidence for a low-velocity channel, interpreted as subducted basaltic crust, to a depth of at least 50–60 km, based on *P-S* converted phases, but is considerably shallower than depths found by *Nakanishi et al.* [1981] and *Matsuzawa et al.* [1986] for a low-velocity channel in the Japanese arc. Either the converted phases sample a different discontinuity or the gabbro-eclogite transition occurs at a different depth beneath Japan. To investigate the Tonga-Kermadec structure further we require instruments situated above the slab in order to detect a waveguide effect; such an experiment in New Zealand might well be effective in determining the depth to the transition.

Our results have consequences for tomographic studies and waveform studies based on ray theory of Gaussian beams. Strong variations of the structure across the slab cause the breakdown of ray theory and related asymptotic methods. Conclusions drawn about the structure of the slab from ray-geometric methods, including some based on Gaussian beams, may therefore be wrong. The results of *Ha* [1978], using Gaussian beam theory, may predict the amplitude of the arrival accurately but do not predict the frequency dependence. However, *Cormier*'s [1989] method is capable of predicting dispersion.

There are also implications for tomographic inversions. The residuals for these events at New Zealand stations are very large and will be omitted from any tomographic study, most of which remove "outliers" of more than a few seconds. Many tomographic studies also use station corrections and New Zealand sites have large corrections for azimuths along the Tonga-Kermadec trench. There is therefore a danger that slab effects will be mapped elsewhere in the mantle: the information on deep structure comes mainly from deep events, all of which reside in subduction zones, all of which have anomalous structure. Tomographic studies, such as those by *Creager and Jordan* [1984] using a coarse parameterization, or even those of *Spakman* [1988], cannot represent a 10 km fast layer nor, in some cases, a 60 km thick lithosphere. It is generally hoped that a coarse parameterisation, combined with a restriction to 1 Hz frequency, eliminates the effects of small-scale structure, but there is no guarantee of this, particularly when ISC data is used without examining the original seismograms for their frequency content. The presence of thin slabs will also give the appearance of anisotropy, with rays traveling in the slab yielding faster times than those traveling across the slab. Coarse sampling of such a structure can easily (and erroneously) be interpreted as evidence for anisotropy.

APPENDIX: DERIVATION OF THE PERIOD EQUATION FOR A HIGH-VELOCITY SLAB

Consider the elastic fluid medium described in section 3. The vertical displacement obeys the wave equation [*Kennett*, 1983]. Consider a plane wave with frequency ω and horizontal wave number k. The vertical slowness in the slab, η_1, is defined by

$$\eta_1^2 = \frac{1}{c_1^2} - \frac{k^2}{\omega^2} \tag{14}$$

with a similar equation for the slowness outside the slab, η_0. In two dimensions (x, z) the vertical motion $w \exp[-i(\omega t - kx)]$ satisfies the equation

$$\frac{\partial^2 w}{\partial z^2} + \eta^2 \omega^2 w = 0 \tag{15}$$

with solutions proportional to $\exp[\pm i\eta\omega z]$.

Let the slab occupy the region between $z = 0$ and $z = H$. We expect leaky modes in the high-velocity slab and represent them with real frequency, allowing the vertical slowness to be complex. The matching conditions at the interfaces $z = 0$ and $z = H$ are continuity of vertical displacement, w, and pressure. The latter condition implies continuity of $(\rho/\eta^2)\ \partial w/\partial z$. The period equation for leaky modes in the slab is obtained by imposing radiation conditions on the upper and lower surfaces: solutions in the infinite medium must take the form of decaying waves traveling away from the slab. Applying continuity of w and pressure and eliminating w_0 gives the conditions

$$\frac{\partial w_1}{\partial z} = \pm i\omega \frac{\eta_1^2}{\eta_0} w_1 \tag{16}$$

where the plus sign is chosen at $z = H$ and the minus sign at $z = 0$, so the waves decay away from the slab.

The general solution in the slab may be written as

$$w_1 = A \cos \omega\eta_1 z + B \sin \omega\eta_1 z \tag{17}$$

where the constants A and B may be complex. Differentiating and substituting into the two matching conditions expressed in (16) gives the period equation for the slowness

$$\begin{vmatrix} i(\eta_1/\eta_0) & \sin\omega\eta_1 H + i(\eta_1/\eta_0)\cos\omega\eta_1 H \\ 1 & i(\eta_1/\eta_0)\sin\omega\eta_1 H - \cos\omega\eta_1 H \end{vmatrix} = 0 \tag{18}$$

which reduces to

$$\tan \omega\eta_1 H = -\frac{2i\eta_0\eta_1}{\eta_0^2 + \eta_1^2}. \tag{19}$$

We define the reduced wave speed d by

$$\frac{1}{d^2} = \frac{1}{c_0^2} - \frac{1}{c_1^2} \tag{20}$$

and the dimensionless parameter γ to replace the (complex) phase speed as

$$\frac{k^2}{\omega^2} = \frac{\gamma}{c_0^2} + \frac{1-\gamma}{c_1^2} \tag{21}$$

so the vertical wave numbers become

$$\eta_0^2 = \frac{1-\gamma}{d^2} \tag{22}$$

and

$$\eta_1^2 = -\frac{\gamma}{d^2} \tag{23}$$

When expressed in terms of γ (19) gives the form of the period equation (1) used in section 4.

Acknowledgments. D.G. thanks the University of Utrecht for support when this work was started. The work was partially supported by NERC grant GR3/7488. We are grateful to Nico Vlaar for numerous discussions and for making us aware of the possible role of the eclogite layer.

REFERENCES

Aki, K., and P. G. Richards, *Quantitative Seismology*, vol. 1, 557 pp., W.H.Freeman and Company, San Francisco, Calif., 1980.

Ansell, J. H., and D. Gubbins, Anomalous high-frequency wave propagation from the Tonga-Kermadec seismic zone to New Zealand, *Geophys. J. R. Astron. Soc.*, *85*, 93–106, 1986.

Bache, T. C., P. D. Marshall, and L. B. Bache, *Q* for teleseismic *P* waves from Central Asia, *J. Geophys. Res.*, *90*, 3575–3587, 1985.

Bretherton, F. P., Propagation in slowly varying waveguides, *Proc. R. Soc. London, Ser. A*, *302*, 555–576, 1968.

Cormier, V. F., Slab diffraction of *S* waves, *J. Geophys. Res.*, *94*, 3006–3024, 1989.

Creager, K. C., and T. H. Jordan, Slab penetration into the lower mantle, *J. Geophys. Res.*, *89*, 3031–3049, 1984.

Davies, D., and B. R. Julian, A study of short-period P-wave signals from Longshot, *Geophys. J. R. Astron. Soc.*, *29*, 185–202, 1972.

Davies, D. and D. P. McKenzie, Seismic travel time residuals and plates, *Geophys. J. R. Astron. Soc.*, *18*, 51–63, 1969.

Der, Z. A., W. D. Rivers, T. W. McElfresh, A. O'Donnell, P. J. Klouda, and M. E. Marshall, Worldwide variations in the attenuative properties of the upper mantle as determined from spectral studies of short-period body waves, *Phys. Earth Planet. Inter.*, *30*, 12–25, 1982.

Dziewonski, A. M., S. Bloch, and M. Landisman, A technique for the analysis of transient seismic signals, *Bull. Seismol. Soc. Am.*, *59*, 427–444, 1969.

Engdahl, E. R., and D. Gubbins, Simultaneous travel time inversion for earthquake location and subduction zone structure in the Central Aleutian Islands, *J. Geophys. Res.*, *92*, 13,855–13,862, 1987.

Fuchs, K., and G. Muller, Computation of synthetic seismograms with the reflectivity method and comparison with observations, *Geophys. J. R. Astron. Soc.*, *23*, 417–433, 1971.

Fukao, Y., K. Kanjo, and I. Nakamura, Deep seismic zone as an upper mantle reflector of body waves, *Nature*, *272*, 606–608, 1978.

Giardini, D., and J. H. Woodhouse, Deep seismicity and modes of deformation in Tonga subduction zone, *Nature*, *307*, 505–509, 1984.

Gilbert, F., and G. E. Backus, Propagator matrices in elastic wave and vibration problems, *Geophysics*, *31*, 326-332, 1966.

Ha, J., A parabolic propagation model for the propagation of precursory signals through the subducted lithosphere, MSc thesis, Victoria Univ., Wellington, New Zealand, 1978.

Helffrich, G. R., S. Stein, and B. J. Wood, Subduction zone thermal structure and mineralogy and their relationship to seismic wave reflections and conversions at the slab/mantle interface. *J. Geophys. Res.*, *94*, 753–763, 1989.

Hori, S., H. Inoue, Y. Fukao, and M. Ukawa, Seismic detection of the untransformed "basaltic" oceanic crust subducting into the mantle, *Geophys. J. R. Astron. Soc.*, *83*, 169–197, 1985.

Huppert, L. N. and C. Frohlich, The P velocity within the Tonga Benioff Zone determined from traced rays and observations, *J. Geophys. Res.*, *86*, 3771–3782, 1981.

Kennett, B. L. N., *Seismic Wave Propagation in Stratified Media*, 342 pp., Cambridge University Press, New York, 1983.

Matsuzawa, T., N. Umino, A. Hasegawa, and A. Takagi, Upper mantle velocity structure estimated from *PS*-converted wave beneath the north-eastern Japan Arc, *Geophys. J. R. Astron. Soc.*, *86*, 767–787, 1986.

McKenzie, D. P., Finite deformation during fluid flow, *Geophys. J. R. Astron. Soc.*, *58*, 689–715, 1979.

Nakanishi, I., Precursors to *ScS* phases and dipping interface in the upper mantle beneath southwestern Japan, *Tectonophysics*, *69*, 1–35, 1980.

Nakanishi, I., K. Suyehiro, and T. Yokota, Regional variations of amplitudes of *ScSp* phases observed in the Japanese Islands, *Geophys. J. R. Astron. Soc.*, *67*, 615–634, 1981.

Ringwood, A. E., Phase transformations and differentiation in subducted lithosphere: Implications for mantle dynamics, basalt petrogenesis, and crustal evolution, *J. Geol.*, *90*, 611–643, 1982.

Sleep, N. H., Teleseismic *P*-wave transmission through slabs, *Bull. Seismol. Soc. Am.*, *63*, 1349–1373, 1973.

Snoke, J. A., I. S. Sacks, and H. Okada, Determination of the subducting lithosphere boundary by use of converted phases, *Bull. Seismol. Soc. Am.*, *67*, 1051–1060, 1977.

Spakman, W., Upper mantle delay time tomography, *PhD thesis*, Univ. of Utrecht, Utrecht, Netherlands, 1988.

Spencer, C. P., and D. Gubbins, Travel-time inversion for simultaneous earthquake location and velocity structure determination in laterally varying media, *Geophys. J. R. Astron. Soc.*, *63*, 95–116, 1980.

Vidale, J. E., Waveform effects of a high-velocity, subducted slab, *Geophys. Res. Lett.*, *14*, 542–545, 1987.

Vidale, J. E., and D. Garcia-Gonzales, Seismic observations of a high velocity slab 1200–1600 km in depth, *Geophys. Res. Lett.*, *15*, 369–372, 1988.

Watson, T. H., A real frequency, complex wave-number analysis of leaking modes, *Bull. Seismol. Soc. Am.*, *62*, 369–384, 1972.

D. Gubbins, Department of Earth Sciences, University of Leeds, Leeds LS2 9JT, United Kingdom.

R. Snieder, Department of Theoretical Geophysics, University of Utrecht, Budapestlaan 4, Utrecht, Netherlands 3508 TA.

(Received March 28, 1990;
revised August 2, 1990;
accepted November 5, 1990.)